COMMUNICATION

Beyond 11% Efficiency: Characteristics of State-of-the-Art $Cu_2ZnSn(S,Se)_4$ Solar Cells

*Teodor K. Todorov, Jiang Tang, Santanu Bag, Oki Gunawan, Tayfun Gokmen, Yu Zhu, and David B. Mitzi**

Widespread adoption of solar energy has the potential to bring human civilization greater long-term economic and geopolitical sustainability than currently possible with fossil fuels. However, to fabricate the needed photovoltaic module capacity beyond terawatt levels it is critical to develop low-cost high-throughput production technologies that are unlimited by materials supply and that yield competitive efficiency levels. Thin-film chalcogenide photovoltaic (PV) technologies offer exceptional opportunity for high-performance, large-area module production, with advantages including the direct band gap absorber, relatively benign grain boundaries with respect to photocarrier recombination and suitability of the technologies for monolithic integration. Indeed, commercial production of the two leading thin-film technologies, CdTe and $Cu(In,Ga)(S,Se)_2$ (CIGSSe), has rapidly increased, with both technologies surpassing 1 gigawatt (GW) production capacity in 2011.[1] Recent performance enhancements in $Cu_2ZnSn(S_{1-x}Se_x)_4$ (CZTSSe) devices, in which the indium and gallium from CIGSSe are replaced by the more abundant and lower cost zinc and tin, have pointed to the possibility of an additional technology that is more readily scalable to >100 GW production capacity – a level that would be required for thin-film PV to ultimately impact rapidly growing world-wide electricity demand, which is currently at 10 TW.[2–11]

CZTSSe (kesterite-type crystal structure) solar cells were first reported in 1996, with 0.66% power conversion efficiencies for the initial vacuum-deposited devices.[2] Subsequent optimization of vacuum-based approaches (using both evaporation and sputtering) led to performance improvement to the 6.7% level by 2008.[9] In 2010, a hydrazine-based deposition process was announced that enabled preparation of a 9.7% kesterite device (further improved to 10.1% in 2011), thereby providing the current benchmark for CZTSSe device development and demonstrating the potential of solution-based processing to, not only compete with vacuum-deposition approaches with regards to cost, but also to excel in terms of performance.[3–5] Despite these developments, the key question remains as to how high the efficiency can improve in CZTSSe[10,11]– i.e., whether this technology is truly a lower cost and earth abundant "drop in replacement" for CIGSSe,[7] with expectations to reach the same 15+% efficiency levels, or whether there are fundamental barriers to the performance based on unique materials properties. Some materials issues that have already been identified include a narrow phase stability field,[12–14] facile evaporation of Sn during heat treatment (i.e., difficulty controlling stoichiometry and phase purity),[15,16] and a range of potentially detrimental defects (e.g., Zn_{Cu}, Cu_{Zn}).[12,17] These and other likely materials issues manifest themselves in the device characteristics as reduced open circuit voltage and higher series resistance (reduced fill factor) compared to analogous CIGSSe devices.[10,11]

In this communication, a series of new record hydrazine-processed CZTSSe devices are reported, all with power conversion efficiency above 10.1% and with the highest certified power conversion efficiency at the 11.1% level, a 10% improvement over the previous benchmark. **Figure 1**a,b shows top view and cross sectional SEM images for one of the high-performance CZTSSe films prepared (see Experimental Section) for the current generation of devices, demonstrating large-grain structure, with some grains extending the full thickness of the CZTSSe layer. Large grains generally benefit device performance because of less opportunity for recombination of photogenerated carriers at the grain boundaries. As is evident in the figure and also noted in earlier work,[3–5] voids at the back contact are still sometimes observed in this generation of devices. The large grain structure is further reflected in the TEM image of Figure 1c for the champion cell film (**Table 1**, device C1). Also evident in this figure is the moderate thickness Mo-Se interfacial layer that forms between the Mo substrate and CZTSSe absorber layer (~200 nm thickness), significantly thinner than our previous reports.[3–5] The Mo-Se interfacial layer impacts both the CZTSSe film adhesion and the ohmic nature of the back contact. In Figure 1d, uniform compositional distribution for all major elements as well as low sulfur content is reflected in the EDX scan across the film. While the high performance films predominantly appear to be homogeneous throughout the bulk of the film, the presence of binary and ternary Cu, Zn and Sn chalcogenides has also been detected in isolated areas, highlighting the significance of the narrow kesterite phase stability region within the Cu-Zn-Sn-S-Se phase diagram and pointing to one area of potential further optimization.

Device characteristics for six of the top-performing CZTSSe devices (cells C1-C6) are presented in Table 1. Note that devices C5 and C6 were each prepared in independent device runs from devices C1-C4. For comparison, we also include data for a previous generation CZTSSe cell (B1) with the same band gap.[3–5] The detailed light/dark *J–V* characteristics and internal quantum efficiency (IQE) data, given as IQE = EQE/(1-*R*), where EQE is the external quantum efficiency and *R* is

Dr. T. K. Todorov, Dr. J. Tang, Dr. S. Bag, Dr. O. Gunawan, Dr. T. Gokmen, Dr. Y. Zhu, Dr. D. B. Mitzi
IBM T. J. Watson Research Center,
P. O. Box 218, Yorktown Heights, NY 10598
E-mail: dmitzi@us.ibm.com

DOI: 10.1002/aenm.201200348

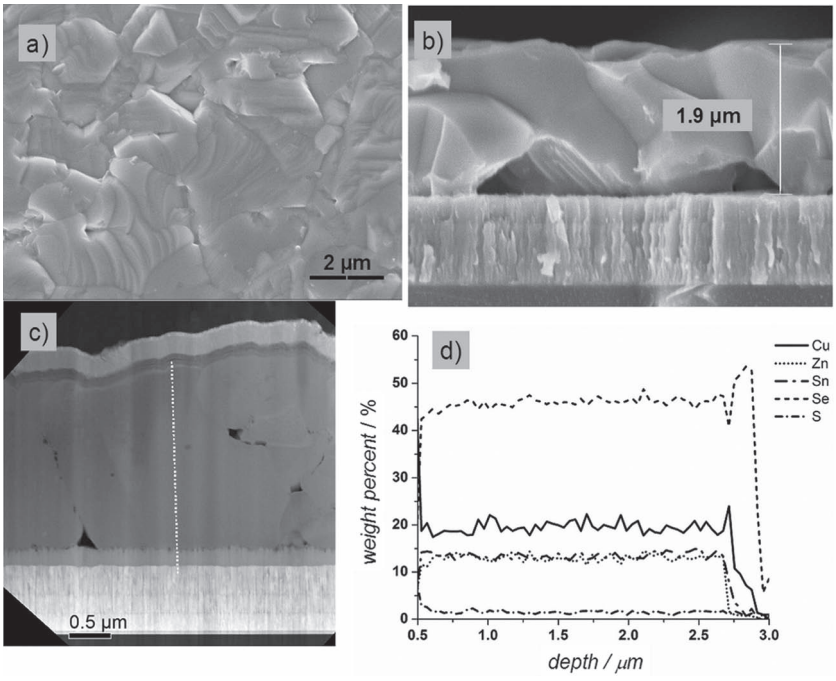

Figure 1. SEM images of the surface (a) and cross section (b) of a CZTSSe film on Mo-coated glass, prepared during the same run as the film used for device C5 (device labeling given in Table 1). TEM image of champion completed device C1 film (c) with corresponding EDX scan taken along the dotted line (d).

the reflectivity, are further presented for the champion device in **Figure 2**. The quantum efficiency (QE) data allow us to estimate the band gap of the absorber layer from the absorption edge using the inflection of the IQE curve (i.e. the peak of the dIQE/dE curve, where $E = hc/\lambda$) near the band edge,[18] as shown in the Figure 2b. The band gaps of most of the champion cells (C1-C5) are determined to be 1.13 eV, which is near the optimum value for the analogous CIGSSe materials family (1.14 eV) and is also close to the value for our previous champion CZTSSe device (1.15 eV).[4,19] Note that for the lower band gap (1.09 eV) device C6, essentially the same 11% (i.e., 10.8%) efficiency can be achieved.

The QE data has a weak decay in the long wavelength region beyond the band edge. Usually, this weak decay is interpreted as a short minority carrier diffusion length. However, the reverse biased EQE at –1 V shows almost identical results with the no bias case, indicating a relatively long carrier diffusion length compared to the depletion width. Therefore, it is suggestive that the observed weak decay in the QE may be due to another factor, such as spatial inhomogeneity of the absorber layer. Assuming that the inhomogeneity is in the form of band gap fluctuations with a Gaussian distribution, the average fluctuation amplitude can be estimated as ~80 meV.[20] Although inhomogeneity on micron and sub-micron scale is expected to be important for device performance, inhomogeneity can be detected even on the millimeter scale for the current generation of devices using light-beam-induced current (LBIC) measurement (**Figure 3**). We observe a photocurrent distribution with standard deviation of ~5% (with respect to the mean value) for the champion cell (C1). This inhomogeneity could arise from bandgap variation across the cell.

From the data in Table 1, improvement in the current generation of CZTSSe devices mainly stems from enhanced fill factor (FF) and short circuit current (J_{sc}). The open circuit voltage V_{oc}, based on the V_{oc} deficit with respect to band gap, E_g/q-V_{oc} (Table 1), does not improve substantially at room temperature relative to earlier generations of CZTSSe devices. However further investigation of the temperature dependence of the V_{oc} for cell C1 (similar behavior is noted for devices C2-C6), as shown in **Figure 4**, presents a notable difference. The V_{oc} vs. temperature plot provides information about the activation energy of the main recombination process, E_A, according to:[21]

$$Voc = E_A/q - AkT/q \times \ln(J_{00}/J_L),$$

Table 1. Device characteristics of the high performance CZTSSe cells (C1-C6) compared to a previous generation CZTSSe device (B1) with similar band gap.

Cell	Eff	FF	V_{oc}	J_{sc}	R_{SL}[a)]	A[a)]	E_g	E_g/q-V_{oc}
	%	%	mV	mA cm^{-2}	Ω cm^2		eV	V
C1	11.1*	69.8*	459.8*	34.5*	0.40	1.5 (1.3)	1.13	0.670
C2	10.8*	68.7*	456.9*	34.4*	0.60	1.6 (1.3)	1.13	0.673
C3	10.9	66.6	468.8	35.0	0.55	1.7 (1.3)	1.13	0.661
C4	10.6	67.0	469.6	33.8	0.47	1.7 (1.3)	1.13	0.660
C5	11.1	69.7	460.6	34.6	0.52	1.6 (1.2)	1.13	0.669
C6	10.8	62.7	447.4	38.6	0.76	2.0 (1.3)	1.09	0.643
B1	9.5	64.4	449.6	32.8	0.50	1.8 (1.4)	1.13	0.680

*Values measured and certified by Newport; [a)] R_{SL} and A are the series resistance and ideality factor determined from light J–V data using Sites' method.[22] The values in parentheses are determined using J_{sc}–V_{oc} data.[27]

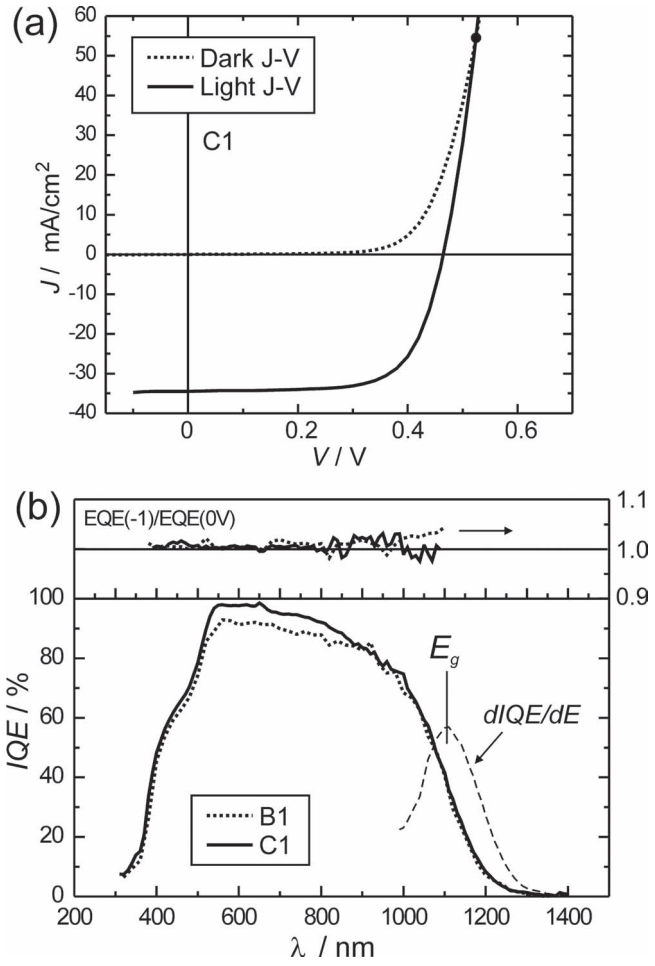

Figure 2. (a) *J–V* characteristics for the 11.1% champion cell C1. (b) Internal quantum efficiency (*IQE*) and the external quantum efficiency (*EQE*) bias ratio *EQE*(−1V)/*EQE*(0V) (top panel) of the champion cell and of the previous generation cell B1.

where A, J_{00} and J_L are the diode ideality factor, reverse saturation current prefactor and the photocurrent, respectively. The 0 K intercept of the linear extrapolation of the high temperature (240 K < T < 340 K) V_{oc} curve yields E_A. Compared to cell B1, we observe that C1 has a higher E_A value, closer to the absorber band gap. Note that in high performance thin film solar cells like CIGSSe and CdTe, E_A matches the absorber band gap value, E_g,[22,23] indicating that the main recombination mechanism is the Schottky-Read-Hall recombination process in the depletion region. Additional recombination processes, such as buffer/absorber interface recombination, can lower E_A. The smaller difference between E_A and E_g for the new generation CZTSSe cells may suggest a reduction in these recombination processes. Interestingly, a boost in the short to medium wavelength (520–900 nm) IQE response is also observed (Figure 2b), which could occur if interface recombination has been reduced. This improvement translates to higher J_{sc} in the new generation of devices.

Fill factor (FF) represents another area of improvement for the current CZTSSe devices, as shown in Table 1. Increased FF is also accompanied by a higher cross over point between the dark and light *J–V* curves, as shown in Figure 2a, which for cell C1 occurs at J = 54 mA cm^{-2}. For cell B1 (typical of previous generation devices), this crossover occurs at a significantly lower (e.g., J < 30 mA cm^{-2}) value. This behavior is also consistent with the better (lower) ideality factors in cells C1 to C5 (A = 1.5 to 1.7, obtained from light *J–V* analysis using Sites' method)[22] compared to cell B1 (A~1.8). Overall, the *J–V* characteristics of the current champion CZTSSe cells are trending towards those for high performance hydrazine-processed CIGSSe devices in terms of diode ideality factor, light/dark *J–V* cross over point, short circuit current, series resistance and fill factor, as the power conversion efficiency is improved.[23] Nevertheless, unlike CIGSSe devices, in addition to the previously discussed open circuit voltage deficit at room temperature, we also still observe a collapse of efficiency at low temperature as shown in **Figure 5**, which is attributed to the increase in series resistance.[10,11] Based on an admittance spectroscopy study in CZTSSe, the apparent divergence of the series resistance at low temperature primarily arises from a carrier freeze out effect due to the lack of a shallow acceptor in the CZTSSe absorber (in contrast, CIGS has a shallow acceptor due to copper vacancies, V_{Cu}).[24] While this issue seems to primarily negatively impact the FF at low temperature, it may impact the room temperature FF as well.

Minority carrier lifetime for the CZTSSe layers can be measured using time-resolved photoluminescence (TRPL) measurement, as shown in **Figure 6** for the champion cell. The decay curves, which do not follow a simple mono-exponential decay, can be modeled by the rate equation that takes into account both linear and quadratic recombination processes.[25] However, even when the quadratic recombination processes are taken into account, the TRPL data cannot be adequately fitted with a single lifetime and lifetimes ranging from 5–8 ns for the 1.13 eV devices (9–14 ns for the 1.09 eV C6 device) are obtained as the time scale increases. The observed bending in the TRPL spectrum may be understood once the prospective spatial inhomogeneity of the samples is taken into account (i.e., see discussion above regarding the QE data), with the measured TRPL signal having individual contributions from different regions with varying lifetimes. Alternatively, since the luminescence originates from a sub-band gap energy, as described below, the TRPL signal may be sensitive to trapping processes in the tail states, which could also give rise to TRPL decay with different lifetimes.

The TRPL data is taken from the peak of the PL spectrum at E = 1.02 eV (see Figure 6 inset). This value is less than the band gap of the absorber layer (E_g = 1.13 eV) as determined from the QE data. Although this may suggest a dominant band to impurity (or band tail) radiative recombination channel contributing to the PL emission, it is also possible that this difference may result from inhomogeneity in the absorber, with the PL spectrum being dominated by the region luminescing at the lowest energy,[25] whereas the QE is a more spatially averaged quantity. In order to observe such a shift in the PL spectrum with respect to the average band gap, the diffusion length should exceed the length scale of the fluctuations.[26]

In summary, we have demonstrated for the first time the possibility of CZTSSe PV technology to reach power conversion efficiencies beyond 11%. The performance improvement

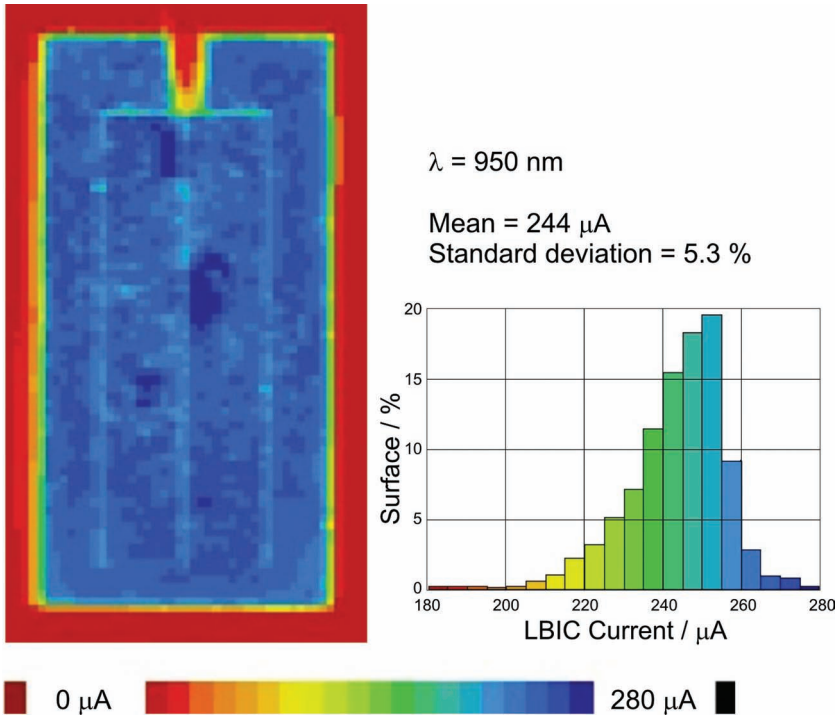

Figure 3. LBIC image of the champion cell C1 using $\lambda = 950$ nm laser excitation. The histogram and the statistics are calculated only from the interior of the cell. A slightly higher photocurrent region (dark blue) is apparent at the center.

relative to previous reports is mainly due to enhanced fill factor and short-circuit current. The crossover behavior between light and dark current-voltage curves is less pronounced and the V_{oc} temperature dependence more closely matches that in high-performance CIGS devices. Nevertheless, the room temperature open circuit voltage deficit remains approximately the same as in previous device generations and represents the primary outstanding issue to address in order to push CZTSSe PV performance further toward the levels achievable in record CIGS devices. Additionally, the divergence in the series resistance and resulting collapse of the power conversion efficiency at low temperature, presumably due to the absence of a shallow acceptor in the CZTSSe system (and resulting carrier freeze out), remains prevalent in the current devices. Despite these issues, the reported progress in room temperature power conversion efficiency continues to point towards a promising future for CZTSSe device technology.

Experimental Section

The CZTSSe absorbers for this study were produced by a hydrazine solution-based process that has been described in detail elsewhere.[3–5] *Caution: Hydrazine is both highly toxic and reactive and must be handled using appropriate protective equipment to prevent physical contact with either vapor or liquid.* Multiple layers of the constituent elements in such solutions were spin coated onto Mo-coated soda lime glass and then heat treated at temperatures in excess of 500 °C. Varying the concentration of sulfur in the atmosphere during the final heat treatment provides a mechanism for controlling the band gap in the resulting film. In this manner well-formed CZTSSe films were produced with thicknesses and band gaps in the range of 1.5–2.2 μm and 1.08–1.12 eV, respectively. Devices were completed using a chemical bath deposited CdS buffer and RF magnetron sputtered ZnO and indium tin oxide (ITO) window layers. A Ni–Al collection grid and ~110-nm-thick MgF_2 antireflection coating were deposited on top of the device by electron-beam evaporation. Each device had a total area of approximately 0.45 cm^2 as defined by mechanical scribing, yielding a standard glass/Mo/CZTSSe/CdS/ZnO/ITO/Ni-Al solar cell.[3–5]

Scanning electron microscopy (SEM) was conducted on the CZTSSe films and devices, which were cleaved prior to the SEM analyses and coated with a thin Pd–Au film to prevent charging effects. Samples for scanning transmission electron microscopy (TEM/STEM) analysis were prepared using a FEI Helios 400 S DB-FIB. TEM images were taken

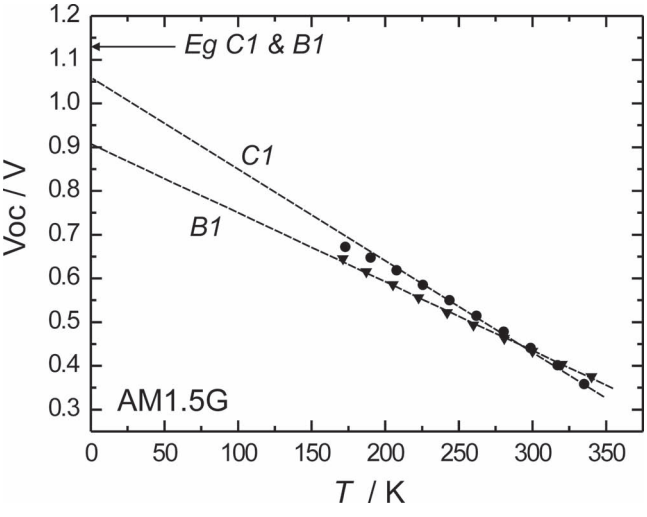

Figure 4. V_{oc} vs temperature data for devices C1 and B1.

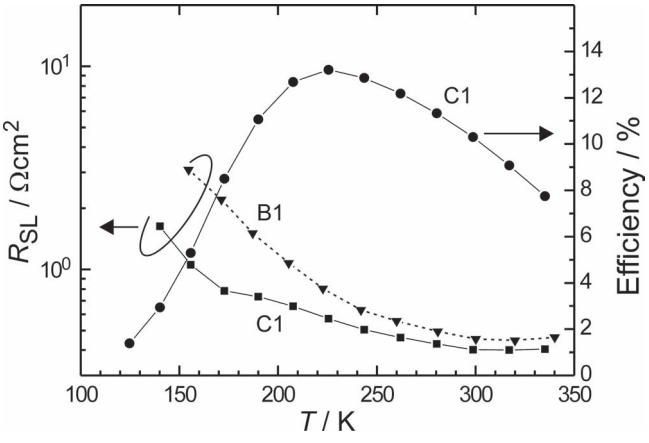

Figure 5. Temperature dependence of the series resistance under light illumination (determined using Sites' method;[22] left axis) and the efficiency (right axis) for devices C1 and B1.

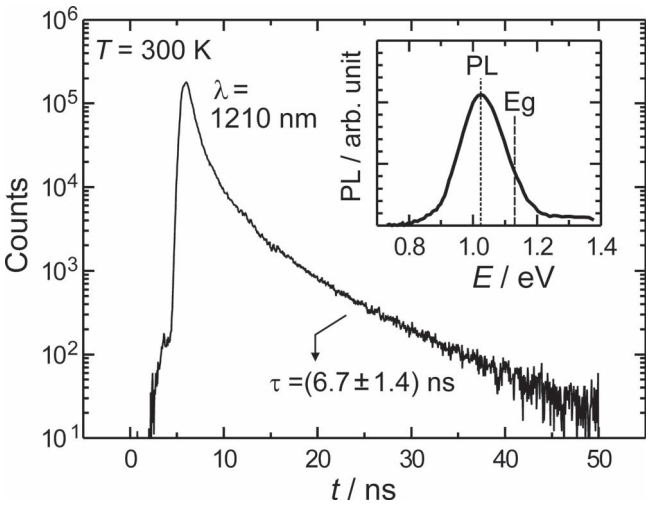

Figure 6. Time-resolved photoluminescence (PL) for device C1. Inset: The PL spectrum, with a peak that occurs at a smaller energy value than the bandgap (as determined from the EQE curve).

using a JEOL 3000F TEM operated at 300 kV. Compositional profiles were acquired by STEM/EDX (energy dispersive X-ray spectroscopy). Light-beam-induced current (LBIC) measurement was conducted using a Semilab WPT-2000 PV system with 125 µm step size. The time-resolved photoluminscence (TRPL) measurement was performed on a finished cell using a Hamamatsu time-correlated single photon counting system. The system employed a 532 nm solid-state laser with a pulse width of less than 1 ns and a repetition rate of 15 kHz. Current density-voltage (*J–V*) characterization for the solar cells was performed using a Xe-based light source solar simulator, equipped with light stabilization system, to provide simulated 1 sun AM1.5G illumination. The 1 sun intensity level was calibrated with a standard Si reference cell, traceable to the National Renewable Energy Laboratory. The quantum efficiency and reflectance measurements were performed using a Protoflex QE1400 system. Solar cell characteristics for our best device were certified by Newport Corporation (Cert#. 524, February 24, 2012). The Newport Technology & Applications Center–PV Lab is certified by the American Association for Laboratory Accreditation (A2LA) as complying with the international consensus standard ISO/IEC 17025. The certified device power conversion efficiency measured by Newport agreed to within 0.1% (absolute) with the value measured in-house.

Acknowledgements

The authors thank S. Thiruvengadam and A. Bhagat for help with substrate preparation, S. Jay Chey and R. Drake for deposition of ZnO and ITO, R. Ferlita for Ni/Al and MgF_2 evaporation, S. Mahajan for area measurement, Jemima Gonsalves for TEM sample preparation. This work was conducted as part of a joint development project between Tokyo Ohka Kogyo Co., Ltd., DelSolar Co., Ltd., Solar Frontier K. K. and IBM Corporation.

Received: May 15, 2012
Revised: June 25, 2012
Published online: August 16, 2012

[1] Solar Frontier press release, Japan's Largest Solar Panel Factory Reaches Full Commercial Operations, Announces Solar Frontier, July 29, 2011, http://www.solar-frontier.com/eng/news (accessed July 2012); First Solar presentation, First Solar, Inc. Announces 2011 Fourth Quarter Financial Results, February 28, 2012, http://investor.firstsolar.com (accessed July 2012).
[2] H. Katagiri, *Tech. Dig. Photovoltaic Sci. Eng. Conf.* Miyazaki, **1996**, *9*, 745.
[3] T. K. Todorov, K. B. Reuter, D. B. Mitzi, *Adv. Mater.* **2010**, *22*, E156.
[4] D. A. R. Barkhouse, O. Gunawan, T. Gokmen, T. K. Todorov, D. B. Mitzi, *Prog. Photovoltaics* **2012**, *20*, 6.
[5] S. Bag, O. Gunawan, T. Gokmen, Y. Zhu, T. K. Todorov, D. B. Mitzi, *Energy Environ. Sci.* **2012**, *5*, 7060.
[6] Q. Guo, G. M. Ford, W. C. Yang, B. C. Walker, E. A. Stach, H. W. Hillhouse, R. Agrawal, *J. Am. Chem. Soc.* **2010**, *132*, 17384.
[7] I. Repins, C. Beall, N. Vora, C. DeHart, D. Kuciauskas, P. Dippo, B. To, J. Mann, W. C. Hsu, A. Goodrich, R. Noufi, *Sol. Energy Mater. Sol. Cells* **2012**, *101*, 154.
[8] B. Shin, O. Gunawan, N. Bojarczuk, S. Guha, *Prog. Photovoltaics* **2012**, DOI: 10.1002/pip.1174.
[9] H. Katagiri, K. Jimbo, S. Yamada, T. Kamimura, W. S. Maw, T. Fukano, T. Ito, T. Motohiro, *Appl. Phys. Expr.* **2008**, *1*, 041201.
[10] O. Gunawan, T. K. Todorov, D. B. Mitzi, *Appl. Phys. Lett.* **2010**, *97*, 233506.
[11] D. B. Mitzi, O. Gunawan, T. K. Todorov, K. Wang, S. Guha, *Sol. Energy Mater. Sol. Cells* **2011**, *95*, 1421.
[12] A. Nagoya, R. Asahi, R. Wahl, G. Kresse, *Phys. Rev. B* **2010**, *81*, 113202.
[13] I. D. Olekseyuk, I. V. Dudchak, L. V. Piskach, *J. Alloy Compd.* **2004**, *368*, 135.
[14] I. V. Dudchak, L. V. Piskach, *J. Alloy Compd.* **2003**, *351*, 145.
[15] J. J. Scragg, T. Ericson, T. Kubart, M. Edoff, C. Platzer-Björkman, *Chem. Mater.* **2011**, *23*, 4625.
[16] A. Redinger, D. M. Berg, P. J. Dale, S. Siebentritt, *J. Am. Chem. Soc.* **2011**, *133*, 3320.
[17] S. Chen, J. H. Yang, X. G. Gong, A. Walsh, S. H. Wei, *Phys. Rev. B* **2010**, *81*, 245204.
[18] S. Merdes, B. Johnson, R. Sáez-Araoz, A. Ennaoui, J. Klaer, I. Lauermann, R. Mainz, A. Meeder, R. Klenk, *Mater. Res. Soc. Symp. Proc.* **2009**, *1165*, M05.
[19] M. A. Contreras, K. Ramanathan, J. AbuShama, F. Hasoon, D. L. Young, B. Egaas, R. Noufi, *Prog. Photovoltaics* **2005**, *13*, 209.
[20] T. Gokmen et al., unpublished.
[21] V. Nadenau, U. Rau, A. Jasenek, H. W. Schock, *J. Appl. Phys.* **2000**, *87*, 584.
[22] J. R. Sites, P. H. Mauk, *Sol. Cells* **1989**, *27*, 411.
[23] T. K. Todorov, O. Gunawan, T. Gokmen, D. B. Mitzi, *Prog. Photovoltaics* **2012**, DOI: 10.1002/pip.1253.
[24] O. Gunawan, T. Gokmen, C. W. Warren, J. D. Cohen, T. K. Todorov, D. A. R. Barkhouse, S. Bag, J. Tang, B. Shin, D. B. Mitzi, *Appl. Phys. Lett.* **2012**, *100*, 253905.
[25] B. Ohnesorge, R. Weigand, G. Bacher, A. Forchel, W. Riedl, F. H. Karg, *Appl. Phys. Lett.* **1998**, *73*, 1224.
[26] J. Mattheis, U. Rau, J. H. Werner, *J. Appl. Phys.* **2007**, *101*, 113519.
[27] D. Pysch, A. Mette, S. W. Glunz, *Sol. Energy Mater. Sol. Cells* **2007**, *91*, 1698.